Micro-Doppler signatures of subwavelength nonrigid bodies in motion

V. Kozlov,[1,*] D. Vovchuk,[1] S. Kosulnikov,[1] D. Filonov,[2] and P. Ginzburg[1]
[1]*School of Electrical Engineering, Tel Aviv University, Tel Aviv, 69978, Israel*
[2]*Center for Photonics and 2D Materials, Moscow Institute of Physics and Technology, Dolgoprudny, 141700 Russia*

(Received 14 June 2021; revised 20 July 2021; accepted 2 August 2021; published 25 August 2021)

Motion signatures of nonstationary electromagnetic bodies are imprinted in their scattering spectrum. While the Doppler frequency shift holds information about the velocity of its center of mass, internal degrees of freedom in a nonrigid body, such as rotation and vibration, introduce nontrivial spectral distortions, termed micro-Doppler signatures. Contemporary analytic characterization of such signatures typically neglects subwavelength electromagnetic coupling, which can dominate the scattering signatures of motion. To address this overlooked scattering regime, a theory of moving coupled dipoles is used to model a moving nonrigid body. The method is verified experimentally in the microwave regime, demonstrating remote sensing of subwavelength information. The method can be useful for analyzing and characterizing effects that frequently emerge in radar science, healthcare monitoring, optical manipulation of particles, and many other applications, where remote sensing and classification of motion are important.

DOI: 10.1103/PhysRevB.104.054307

I. INTRODUCTION

The Doppler effect, observed in waves reflected from moving scatterers, has been widely studied and employed for over a century across such diverse fields as astronomy, optics, radar, acoustics, and more. At the heart of the phenomenon is the frequency shift of the echo wave by an amount that is related to the velocity of the moving body, yet the motion of a nonrigid body can be more complex and consist of translational and rotational degrees of freedom for all of its constitutive parts. These in turn contribute to the modulation of the backscattered wave, where the resulting collection of spectral shifts is referred to as the micro-Doppler effect [1]—largely due to the fact that it is often smaller than the main Doppler shift, caused by the linear motion of the center of mass. The micro-Doppler effect was first introduced in coherent laser radar systems where it was easier to observe [2], but with technological improvements it became observable in radar [3] and sonar [4] systems. Today, owing to the fact that the micro-Doppler signatures are object specific, they are extensively used for remote sensing and moving target classification purposes in the radio-frequency regime [5,6], as well as in the optical portion of the electromagnetic spectrum, which is frequently employed to manipulate subwavelength particles, gaining valuable information from their motion signatures [7–10].

The Doppler and, by extension, the micro-Doppler effects are fundamentally nonstationary phenomena, and can therefore produce new frequencies in the scattering spectrum. While addressing electromagnetic interactions with fast moving relativistic bodies is extremely challenging, seeing as both Maxwell's equations and the material constitutive relations change in accelerating reference frames [11], nonrelativistic motion can be approached more simply by treating it as a parametric process. In this case, "quasistationary" principles can be applied [12–14]; i.e., the moving body is assumed to be instantaneously stationary in respect to the "fast time" of the excitation, which is characterized by very fast propagation velocity and high field oscillation frequency at any particular time. The scattering problem may then be solved in the same manner as any ordinary time-independent scenario. The next step is to stitch the parametric solutions together forming the so-called "slow time," associated with the slow motion of the body, forming the time-dependent solution. As a stand-alone example it is worth noting a unique interaction regime, where electromagnetic memory within a nonrelativistic body was shown to play a role [10]. The stationary solutions can be obtained via full-wave numerical simulation or with semi-analytical tools, including the discrete dipole approximation (DDA) [15]. This approach, where a complex body is divided into a collection of subwavelength scatterers, allows obtaining intuitive yet accurate solutions of scatting problems, e.g., [1,16–18]. In a nutshell, the formulation is based on self-consistent matrix equations, where polarizabilities are used to calculate the induced dipole moments on each element within the discretized body, therefore allowing the calculation of the scattered fields.

It is quite remarkable that in the radio-frequency community the main contemporary approach for micro-Doppler analysis resembles the DDA, but with one distinctive difference. While the scatterer is subdivided into a grid of cells, considering each cell as a pointlike scatterer, these points are then considered independently and the scattering problem is solved for each cell at a specific point in time without accounting for the coupling between adjacent cells. This procedure is repeated for all cells and those partial contributions to the overall scattering are coherently summed at the observation

*vitaliko@mail.tau.ac.il

point [1,16]. This method, typically applied in radar science, assumes that there is no significant coupling between the different cells and neglects modulation contributed by subwavelength motion. This approach resembles an old radar concept of "trapping centers," where the target is empirically characterized by several points, which are the main contributors to the reflected echoes [19]. For example, it could be a collection of corner reflectors on a ship, or a number of sharp corners on a car. Neglecting the coupling between scattering centers greatly simplifies the analysis and is often justified under conditions of short wavelength illumination or weak scattering regime (e.g., the first Born approximation in a broader sense [20]). Yet this approach is inadequate when coupling becomes significant, such as in the case of long wavelength excitation with subwavelength motion. Typical examples here include motions of subwavelength parts of a rigid body, the blinking eyelids of a pedestrian, a car antenna flapping in the wind, or the rotation of a fan.

It is therefore evident that contemporary analysis is lacking when the moving body is interrogated by long wavelength sources, urging the extension of the DDA to account for quasistationary time-dependent motion of the scattering scene, improving the finesse of remote sensing. Furthermore, if the internal degrees of freedom do not exhibit time-periodic evolution, applying full-wave solutions within the quasistationary approach becomes computationally challenging, while DDA can often be solved analytically in closed form for many simple systems, or at least provide a considerable computational advantage in cases where closed solutions do not exist.

In this paper, a time-dependent coupled dipoles theory is developed and demonstrated experimentally by examining a simple system of two subwavelength rotating scatterers located close to each other. The scatterers are constructed from metal wires (dipoles) illuminated by radar, while rotating with some frequency and with an initial angle with respect to each other. A few cases of interest are considered, discussed, and then verified experimentally, revealing that the scattering phenomena can be strongly affected by near-field coupling in the low frequency regime, primarily encompassed in the appearance of mixed harmonics in the spectra of the scattered field, a phenomenon that cannot be accounted for by the existing treatments of micro-Doppler signatures. While this experiment is conducted in the electromagnetic microwave frequency range, the time-dependent DDA is relevant to all the electromagnetic spectral range, as well as for any other types of waves traveling in an arbitrary medium where bodies can be decomposed using the DDA approach.

II. TIME-DEPENDENT DISCRETE DIPOLE APPROXIMATION

While the proposed theoretical approach can be straightforwardly extended to include multiple degrees of freedom, here we will concentrate on a pair of near-field coupled rotating dipoles, seeing as this simple configuration allows for closed form solutions containing physical intuition into the phenomena. The resulting model will be subsequently tested experimentally.

Consider two dipoles rotating in the z-y plane, separated by a distance d in the x direction, as depicted in Fig. 1. Both

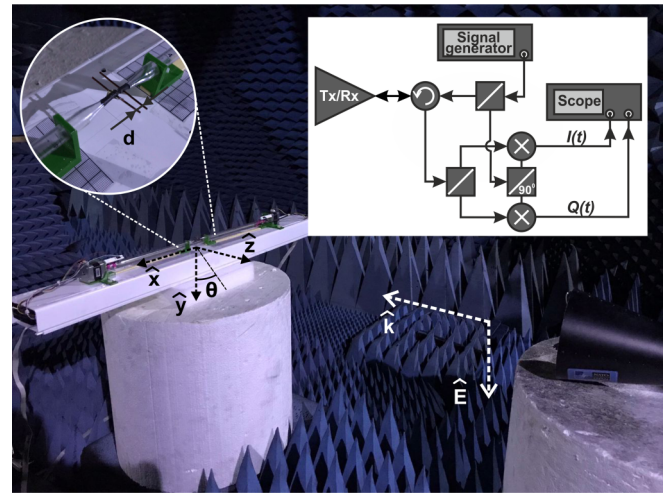

FIG. 1. Experimental setup. A monochromatic wave interacts with two rotating wires. Photo of the experimental setup in an anechoic chamber. (Inset) Scheme of the I/Q demodulator.

dipoles rotate around their center so that the angle between their principal axis and the Z axis as a function of time is given by $\theta_1 = \dot{\theta}_1 t + \theta_{10}, \theta_2 = \dot{\theta}_2 t + \theta_{20}$, where $\dot{\theta}_1, \dot{\theta}_2$ are the angular rotation frequencies of each dipole and θ_{10}, θ_{20} is the initial angle between each dipole and the Z axis at time $t = 0$. The dipoles are illuminated by a plane wave of the form $\bar{E}^i = E_0 e^{jkz}\hat{y}$ (the harmonic time convention throughout the text is $e^{j\omega t}$). Using a coupled dipoles method similar to the one used in [17,21], a self-consistent set of equations for the dipolar electric moments may be written as

$$\begin{aligned} \bar{P}_1 &= \bar{\bar{\alpha}}_1\left(\bar{E}_1^i + \bar{E}_2^s\right), \\ \bar{P}_2 &= \bar{\bar{\alpha}}_2\left(\bar{E}_2^i + \bar{E}_1^s\right), \end{aligned} \tag{1}$$

where $\bar{E}_1^i = \bar{E}_2^i = E_0\hat{y}$, $\bar{E}_1^s = \varepsilon_0^{-1}\bar{\bar{A}}(d)\bar{P}_2$ is the scattered field by dipole 2 at the location of dipole 1 and similarly $\bar{E}_2^s = \varepsilon_0^{-1}\bar{\bar{A}}(d)\bar{P}_1$ is the scattered field of dipole 2 at the location of dipole 1. $\bar{\bar{A}}(d) = \frac{e^{-jkd}}{4\pi d}[(k^2 - \frac{1}{d^2} - \frac{jk}{d})(\hat{y}\hat{y} + \hat{z}\hat{z}) + 2(\frac{1}{d^2} + \frac{jk}{d})\hat{x}\hat{x}]$ is the Green's dyadic and the time-dependent polarizabilities due to the rotational motion are given by [21]

$$\bar{\bar{\alpha}}_i(t) = \begin{pmatrix} 0 & 0 & 0 \\ 0 & \sin^2[\theta_i(t)] & \frac{1}{2}\sin[2\theta_i(t)] \\ 0 & \frac{1}{2}\sin[2\theta_i(t)] & \cos^2[\theta_i(t)] \end{pmatrix}\alpha_i \tag{2}$$

At this point it is important to note that a quasistatic, adiabatic approach is undertaken in the treatment above, where the rotation frequency is considered to be far slower than the frequency of incident field. In this case Fourier analysis is used, while considering the polarizability $\bar{\bar{\alpha}}_i(t)$ as a parameter that changes on a significantly slower timescale (e.g., [13,14]). Equation (1) is a system of linear equations that can be solved by inversion to reveal the time-dependent dipole moment of

each scatterer:

$$\begin{aligned}\bar{P}_1 &= \left[\bar{\bar{I}} - \varepsilon_0^{-2}\bar{\bar{\alpha}}_1\bar{\bar{A}}(d)\bar{\bar{\alpha}}_2\bar{\bar{A}}(d)\right]^{-1}\bar{\bar{\alpha}}_1\left[\bar{E}_1^i + \varepsilon_0^{-1}\bar{\bar{A}}(d)\bar{\bar{\alpha}}_2\bar{E}_1^i\right]\\ \bar{P}_2 &= \left[\bar{\bar{I}} - \varepsilon_0^{-2}\bar{\bar{\alpha}}_2\bar{\bar{A}}(d)\bar{\bar{\alpha}}_1\bar{\bar{A}}(d)\right]^{-1}\bar{\bar{\alpha}}_2\left[\bar{E}_2^i + \varepsilon_0^{-1}\bar{\bar{A}}(d)\bar{\bar{\alpha}}_1\bar{E}_1^i\right],\end{aligned} \tag{3}$$

which under the condition $\alpha_1 = \alpha_2 \equiv \alpha$ simplifies to

$$\begin{aligned}\bar{P}_1 &= \frac{\alpha E_0}{1 - v^2(d)\cos^2(\theta_1 - \theta_2)}\begin{pmatrix}0\\ \cos^2(\theta_1) + v(d)\cos(\theta_1)\cos(\theta_2)\cos(\theta_1 - \theta_2)\\ \cos(\theta_1)\sin[\theta_1(t)] + v(d)\sin(\theta_1)\cos(\theta_2)\cos(\theta_1 - \theta_2)\end{pmatrix},\\ \bar{P}_2 &= \frac{\alpha E_0}{1 - v^2(d)\cos^2(\theta_1 - \theta_2)}\begin{pmatrix}0\\ \cos^2(\theta_2) + v(d)\cos(\theta_1)\cos(\theta_2)\cos(\theta_1 - \theta_2)\\ \cos(\theta_2)\sin[\theta_2(t)] + v(d)\sin(\theta_2)\cos(\theta_1)\cos(\theta_1 - \theta_2)\end{pmatrix},\end{aligned} \tag{4}$$

where $v(d) = \frac{\alpha e^{-jkd}}{4\pi\varepsilon_0 d^3}[dk(dk-j) - 1]$ is the coupling coefficient that depends on the distance d between the dipoles and $\bar{\bar{I}}$ is the unit matrix. Now that the dipole moments are known, the scattered field can be calculated. For a point located at a distance r on the z axis, for example, the scattered field is given by

$$\bar{E}_s(t) = \varepsilon_0^{-1}(\bar{\bar{A}}_{r1}\bar{P}_1 + \bar{\bar{A}}_{r2}\bar{P}_2) \approx \frac{\alpha E_0\varepsilon_0^{-1}A_r[\cos^2(\theta_1) + \cos^2(\theta_2) + 2v(d)\cos(\theta_1)\cos(\theta_2)\cos(\theta_1 - \theta_2)]}{1 - v^2(d)\cos^2(\theta_1 - \theta_2)}\hat{y} \equiv E_s(t)\hat{y}, \tag{5}$$

where in the present geometry the two dyadics transforming the dipolar sources into the far field are approximately ($\frac{d}{r} \ll 1$) equal $\bar{\bar{A}}_{r1} \approx \bar{\bar{A}}_{r2} \approx \frac{e^{-jkr}k^2}{4\pi r}(\hat{x}\hat{x} + \hat{y}\hat{y}) \equiv A_r(\hat{x}\hat{x} + \hat{y}\hat{y})$. By expanding the denominator of Eq. (5) [$v(d) \ll 1$], it becomes evident that a frequency comb is expected to appear in the scattered field, containing frequencies that are combinations of the rotational angular frequencies of the dipoles,

$$E_s(t) = \sum_{n=-\infty}^{\infty}\sum_{m=-\infty}^{\infty}[C_{mn}\cos[(m\dot{\theta}_1 + n\dot{\theta}_2)t] + S_{mn}\sin[(m\dot{\theta}_1 + n\dot{\theta}_2)t]] \tag{6}$$

where the coefficients C_{mn} and S_{mn} can be obtained straightforwardly as will be done ahead for a few cases of interest [$\tilde{E}(\Omega)$ is the slow time Fourier transform of $E_s(t)$].

A. Same direction synchronous rotation: $\dot{\theta}_1 = \dot{\theta}_2$, $\dot{\theta}, \dot{\theta}_{10} = 0, \theta\theta_{20} \equiv \theta_0$

$$|\widetilde{E}_s(\Omega = 2\dot{\theta})| \propto \left|\frac{\cos(\theta_0)}{1 - v\cos(\theta_0)}\right|. \tag{7}$$

In this case the wires rotate together in the same direction and the micro-Doppler spectrum solely depends on the angle between the dipoles. For strong coupling a deviation of the amplitude from the cosine can be observed. When the two dipoles are perpendicular ($\theta_0 = \pi/2$), their micro-Doppler signatures interfere destructively at the observation point, rendering them invisible; i.e., the imprint of motion in this harmonic disappears. This is an expected result seeing as two perpendicular dipoles rotating at the same frequency are invariant to simultaneous rotation by an angle that is an integer multiple of $\pi/2$. This means that the scattered field at the observation point would have periodicity that produces a harmonic at $\Omega = 4\dot{\theta}$. The expansion of Eq. (5) does not predict this harmonic for this case. This is the result of the dipolar approximation, which needs to be extended to higher multipoles to obtain this result [22,23]. This scenario, though, can be considered as a singular point of the theory and is not expected to emerge in any practical situation.

B. Opposite direction synchronous rotation: $\dot{\theta}_1 = -\dot{\theta}_2$, $\dot{\theta}, \theta_{10} = -\theta_{20} \equiv \frac{\theta_0}{2}$

$$\begin{aligned}E_s(t) &\propto \frac{1 + \cos(2\dot{\theta}t + \theta_0)}{1 - v\cos(2\dot{\theta}t + \theta_0)},\\ |\widetilde{E}_s(\Omega = \mathrm{m}\dot{\theta})| &\neq f(\theta_0)\ \forall m,\end{aligned} \tag{8}$$

where the fact that the amplitude is not a function of the initial angle follows from the observation that the temporal scattered field $E_s(t)$ contains θ_0 as a mere shift which therefore only affects the phase of the scattered field. This suggests none of the scattered micro-Doppler harmonics [which can be written down by expansion of the denominator of Eq. (8)] should have amplitude dependence on the initial angle.

C. Asynchronous rotation $\dot{\theta}_1 \neq \dot{\theta}_2$, $\theta_{10} = \theta_{20} = 0$

$$E_s(t) \propto \frac{1 + \frac{1}{2}(1 + v)[\cos(2\dot{\theta}_2 t) + \cos(2\dot{\theta}_2 t)] + \frac{v}{2}\{1 + \cos[2(\dot{\theta}_1 - \dot{\theta}_2)t]\}}{1 - v^2\cos^2[(\dot{\theta}_1 - \dot{\theta}_2)t]}, \tag{9}$$

In this case the nominator reveals that a mixed harmonic of frequency $2(\dot{\theta}_1 - \dot{\theta}_2)$ emerges, the amplitude of which is proportional to the strength of the coupling coefficient $v(d)$. This new frequency is the direct result of the near-field

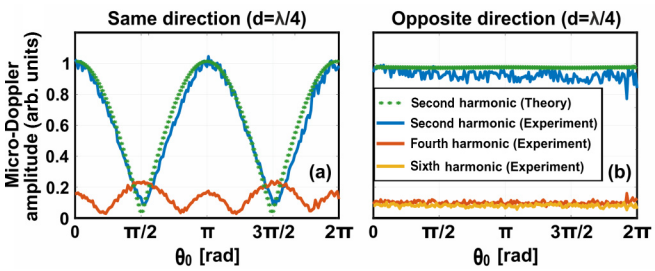

FIG. 2. Comparing the experimental amplitudes of the micro-Doppler harmonics (second, fourth, and sixth) as a function of the initial angle θ_0 between the dipoles, which rotate around the same axis with angular frequency $\dot{\theta}_1 = \dot{\theta}_2 = 16$ rad/s at a distance of $\frac{\lambda}{4}$. The results are compared with the DDA theory for two cases. (a) The dipoles are both rotating in the same direction [Eq. (7)]. (b) The dipoles are rotating in opposite directions [Eq. (8)].

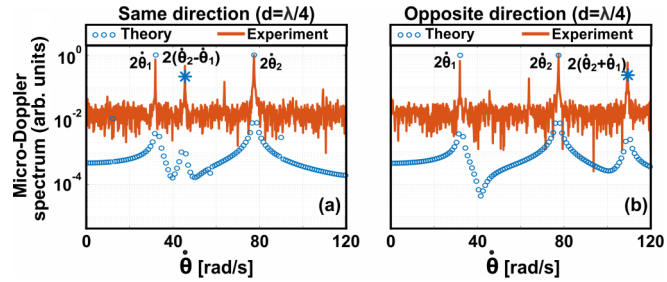

FIG. 3. Comparison between the experimental and DDA theory micro-Doppler combs for two asynchronously ($\dot{\theta}_1 \neq \dot{\theta}_2$) rotating dipoles located at a distance of $\frac{\lambda}{4}$. The angular rotation frequencies are $\dot{\theta}_1 = 16$ rad/s and $\dot{\theta}_2 = 39$ rad/s. (a) Both dipoles rotate in the same direction, producing a sum frequency at $2(\dot{\theta}_2 + \dot{\theta}_1)$. (b) Both dipoles rotate in opposite directions, producing a difference frequency at $2(\dot{\theta}_2 - \dot{\theta}_1)$. Stars indicate the mixed harmonic.

coupling, and depends on whether the two dipoles are rotating in the same direction (producing a difference frequency) or in opposite directions (producing a sum frequency). For strong coupling the denominator of Eq. (9) may be expanded in a similar fashion to Eq. (6), revealing a series of additional mixed harmonics with amplitudes that depend on powers of the coupling coefficient $v(d)$.

III. EXPERIMENTAL VERIFICATION

The experiment was performed in an anechoic chamber, as shown in Fig. 1. The setup consisted of two dipoles made of 40 mm length copper wires, located at a controllable distance d away from each other. The distance was varied between 5 and 65 mm. Both dipoles were allowed to rotate independently around their axis using a stepper motor, controlled by a closed loop system to ensure stable long-time operation. The dipoles were illuminated by a continuous wave at 3.2 GHz (chosen based on the length of the wires). The N5173B phased locked signal generator was connected to a horn antenna, polarized in the rotation plane of the dipoles. The same antenna was used to receive the backscattered field. I/Q demodulation of the echoes with a coherent homodyne scheme was performed [Fig. 1(b)]. The resulting baseband signals were sampled and recorded on a DSOX3104T scope.

The time-dependent signal was processed by applying a complex fast Fourier transform to reveal the micro-Doppler frequency comb, containing harmonics that are multiples of the rotation frequencies of the dipoles, as predicted by Eq. (6). In particular, the second and fourth harmonics were computed in order to validate the theoretical results of Eqs. (7)–(9). Recall that harmonics are related to the angular rotation frequency of the wires and emerge at the baseband of the scattered signal. First, the dependence of the initial angle on these harmonics was inspected by repeating the experiment for various initial angles between the two dipoles before initiating the rotation. The results appear in Fig. 2. It can be seen that for the case of synchronous rotation in the same direction (i.e., $\dot{\theta}_1 = \dot{\theta}_2$), the second harmonic behaves in a periodic manner as a function of the initial angle between the dipoles, as predicted by Eq. (7). As discussed in the text following the derivation of the equation, the fourth harmonic is not well modeled due to the necessity to account for higher multipolar moments. The experimental results show that the fourth harmonic is indeed maximal at $\theta_0 = \pi/2$ as expected. It should also be noted that this periodic dependence on initial angle is not a subwavelength effect; rather it is the result of interference between the scattered fields of each dipole, seeing as the effect should only have weak dependence on the coupling coefficient. Regardless, this result supports the framework of time-dependent DDA. In contrast, when the dipoles are synchronously rotated in opposite directions (i.e., $\dot{\theta}_1 = -\dot{\theta}_2$), no dependence on initial angle is observed in any of the harmonics, in complete agreement with Eq. (8).

Next the dipoles were rotated asynchronously (i.e., $\dot{\theta}_1 \neq \dot{\theta}_2$), while the micro-Doppler spectrum was recorded. In this case too, a distinction between same and opposite directions of rotation can be observed, as shown in Fig. 3. When the dipoles rotate in the same direction, a difference harmonic appears in the spectrum, while a sum harmonic appears when the two rotate in opposite directions, exactly as suggested by Eq. (9). The figure was normalized to the amplitude of the second harmonic of the second dipole, which had slightly higher amplitude than that of the first dipole, owing to slight variations in their length, as well as small deviations from perfect alignment of the antenna. Another experimental feature apparent in Fig. 3 is the fourth micro-Doppler harmonic for the first wire, appearing clearly above noise level at about 64 rad/s. As discussed in Eq. (7), modeling the higher harmonics for quarter wavelength wires requires additional multipoles (or use of the Hallen integral [22]). In addition, the theoretical plot in Fig. 3(a) predicts two more mixed harmonics at 14 and 92 rad/s, corresponding to $2\dot{\theta}_2 - 4\dot{\theta}_1$ and $4(\dot{\theta}_2 - \dot{\theta}_1)$, respectively. However, these additional harmonics are below the noise floor and therefore cannot be observed experimentally.

The appearance of the mixed harmonics is clear indication of coupling between internal degrees of freedom, which is neglected in standard radar analysis. In order to further verify this claim, the amplitude of the various harmonics presented in Fig. 3 has been recorded as a function of the distance between the rotating dipoles and plotted in Fig. 4. It can be seen that in both cases the mixed harmonic decays with distance, while the other harmonics behave in an oscillatory fashion as expected in the case of interfering fields. This result shows the strength

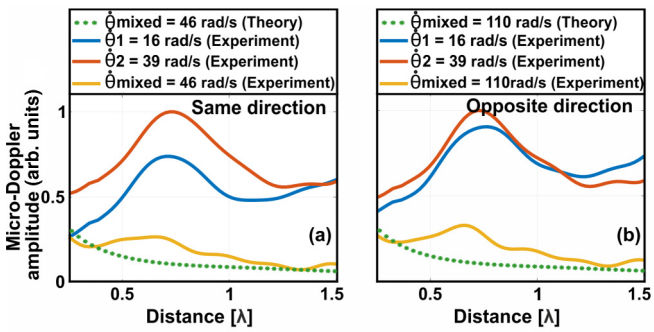

FIG. 4. Experimental validation for the subwavelength coupling origin of the mixed harmonic. The experimental amplitudes of the second and mixed micro-Doppler harmonics are plotted versus distance and compared to the theory. (a) The dipoles are both rotating in the same direction. (b) The dipoles are rotating in opposite directions.

of DDA analysis for remote sensing applications, allowing the extraction of information about the relative direction of rotation between the two subwavelength bodies. Similar analysis for more complex nonrigid body dynamics can help extract additional information that can be used for micro-Doppler based classification and identification.

IV. OUTLOOK AND CONCLUSION

Time-dependent DDA theory had been developed and experimentally tested on an example of two near-field coupled rotating dipoles. It was shown that the coupling between time-dependent degrees of freedom, originated from the motion of constitutive parts of a nonrigid body, plays an important role for long wavelength excitations. Furthermore, under certain conditions, the scattered field spectra might be completely governed by these interactions. As an outlook, the developed formalism can be further extended to consider scattering processes form complex nonrigid bodies. Assuming that the mechanical evolution of a system is known, the structure can be divided into a set of polarizable volumetric cells, interacting with each other. In contrary to static DDA, time-dependent mutual interactions between the cells are taken into account and form the overall response of a nonrigid body. However, the choice of a partition, approximation of coupling coefficients and several other body-specific aspects (e.g., a combination of moving and stationary elements within a structure), remain an open question. Nevertheless, the developed approach, having direct relation to micro-Doppler signatures of radar targets, allows to perform studies of more complex scenarios. Although initially applied to classification of jet engines [24,25] and helicopter rotor blades [26,27], micro-Doppler analysis starts to become a leading motive in many modern applications, including humans detection behind obstacles [28], relevant to rescue operations, autonomous car safety [29], where the different motions of a busy street need to be classified and categorized quickly, and the rapidly growing need to identify unmanned flying drones [30,31]. The method finds extensive use in the optical part of the spectrum where light manipulates subwavelength particles, gaining valuable insight from their signatures of motion [7–10]. Finally, a recent and exciting application concerns hand gesture recognition, aimed at facilitating touchless interaction with computers [32,33]. A quick review of new relevant topics underlines the need of reliable theoretical models in the field. Our investigation is an endeavor in this direction.

ACKNOWLEDGMENTS

The research was supported by ERC StG "In Motion" (Grant No. 802279) and PAZY Foundation (Grant No. 01021248). D.F. acknowledges the Russian Science Foundation under Project No. 20-19-00491 for supporting the experimental part of the work.

[1] V. C. Chen, *The Micro- Doppler Effect in Radar* (Artech House, Boston, 2011).
[2] V. C. Chen, D. Tahmoush, and W. J. Miceli, Radar Micro-Doppler Signature Processing and Applications (IET Digital Library, 2014).
[3] V. C. Chen, Micro-Doppler effect of micromotion dynamics: A review, Proc. SPIE **5102**, 240 (2013).
[4] Z. Zhang, P. Pouliquen, A. Waxmant, and A. G. Andreou, Acoustic micro-Doppler gait signatures of humans, in *41st Annual Conference on Information Sciences and Systems* (IEEE, Piscataway, NJ, 2007), pp. 627–630.
[5] J. Lei, Pattern recognition based on time-frequency distributions of radar micro-Doppler dynamics. 3. Micro-Doppler signature pattern, in *Proceedings of the Sixth International Conference on Software Engineering, Artificial Intelligence, Networking and Parallel/Distributed Computing and First ACIS International Workshop on Self-Assembling Wireless Networks* (IEEE, Washington, DC, 2005).
[6] J. Lei and C. Lu, Target classification based on micro-Doppler signatures, in *Radar Conference, 2005 IEEE International* (IEEE, Washington, DC, 2005), pp. 1–5.
[7] A. Korobenko, A. A. Milner, J. W. Hepburn, and V. Milner, Rotational spectroscopy with an optical centrifuge, Phys. Chem. Chem. Phys. **16**, 4071 (2014).
[8] A. A. Milner, A. Korobenko, J. W. Hepburn, and V. Milner, Effects of Ultrafast Molecular Rotation on Collisional Decoherence, Phys. Rev. Lett. **113**, 043005 (2014).
[9] O. Faucher, E. Prost, E. Hertz, F. Billard, B. Lavorel, A. A. Milner, V. A. Milner, J. Zyss, and I. S. Averbukh, Rotational Doppler effect in harmonic generation from spinning molecules, Phys. Rev. A **94**, 051402 (2016).
[10] A. A. Milner and V. Milner, Controlling the degree of rotational directionality in laser-induced molecular dynamics, Phys. Rev. A **103**, L041103 (2021).
[11] J. G. Van Bladel, *Relativity and Engineering* (Springer, Berlin, 1984).
[12] J. Van Bladel, Electromagnetic fields in the presence of rotating bodies, Proc. IEEE **64**, 301 (1976).
[13] V. Kozlov, S. Kosulnikov, D. Filonov, A. Schmidt, and P. Ginzburg, Coupled micro-Doppler signatures of closely located targets, Phys. Rev. B **100**, 214308 (2019).

[14] V. Kozlov, S. Y. Kosulnikov, D. Vovchuk, and P. Ginzburg, Memory effects in scattering from accelerating bodies, Adv. Photonics **2**, 056003 (2020).

[15] L. Novotny and B. Hecht, *Principles of Nano-Optics* (Cambridge University Press, Cambridge, 2009).

[16] H. W. Victor and C. Chen, Micro-Doppler effect in radar: Phenomenon, model, and simulation study, IEEE Trans. Aerosp. Electron. Syst. **42**, 02 (2006).

[17] V. Kozlov, D. Filonov, A. S. Shalin, B. Z. Steinberg, and P. Ginzburg, Asymmetric backscattering from the hybrid magneto-electric meta particle, Appl. Phys. Lett. **109**, 203503 (2016).

[18] D. Markovich, K. Baryshnikova, A. Shalin, A. Samusev, A. Krasnok, P. Belov, and P. Ginzburg, Enhancement of artificial magnetism via resonant bianisotropy, Sci. Rep. **6**, 22546 (2016).

[19] Y. Chen, *Micro-Doppler Characteristics of Radar Targets* (Elsevier, Amsterdam, 2017).

[20] M. Born and E. Wolf, *Principles of Optics: Electromagnetic Theory of Propagation, Interference and Diffraction of Light*, 7th ed. (Cambridge University Press, Cambridge, 1999).

[21] D. Filonov, B. Z. Steinberg, and P. Ginzburg, Asymmetric micro-Doppler frequency comb generation via magnetoelectric coupling, Phys. Rev. B **95**, 235139 (2017).

[22] V. Kozlov, D. Filonov, Y. Yankelevich, and P. Ginzburg, Micro-Doppler frequency comb generation by rotating wire scatterers, J. Quant. Spectrosc. Radiat. Transfer **190**, 7 (2017).

[23] S. Mühlig, C. Menzel, C. Rockstuhl, and F. Lederer, Multipole analysis of meta-atoms, Metamaterials **5**, 64 (2011).

[24] J. Park, W. Yang, J. Bae, S. Kang, and N. Myung, Extraction of jet engine modulation component weakly present in measured signals for enhanced radar target recognition, J. Electromagn. Waves Appl. **28**, 963 (2014).

[25] H. Lim, N. H. Myung, H. Lim, and N. H. Myung, High resolution range profile-jet engine modulation analysis of aircraft models, J. Electromagn. Waves Appl. **25**, 1092 (2011).

[26] A. Stefanov and S. Member, Helicopter rotor-blade modulation of antenna radiation characteristics, IEEE Trans. Antennas Propag. **49**, 688 (2001).

[27] A. Cilliers and W. A. J. Nel, Helicopter parameter extraction using joint time-frequency and tomographic techniques, in *2008 International Conference on Radar* (IEEE, Washington, DC, 2008), pp. 598–603.

[28] M. Ritchie, M. Ash, Q. Chen, and K. Chetty, Through wall radar classification of human micro-Doppler using singular value decomposition analysis, Sensors **16**, 1401 (2016).

[29] D. Belgiovane and C. Chen, Micro-Doppler characteristics of pedestrians and bicycles for automotive radar sensors at 77 GHz, in *11th European Conference on Antennas and Propagation* (IEEE, PIscataway, NJ, 2017), pp. 2912–2916.

[30] J. Michael, Z. Lu, and V. C. Chen, Experimental study on radar micro-Doppler signatures of unmanned aerial vehicles, in *Radar Conference (RadarConf '17)* (IEEE, Washington, DC, 2017), pp. 854–857.

[31] A. K. Singh and Y.-H. Kim, Automatic measurement of blade length and rotation rate of drone using W-band, IEEE Sens. J. **18**, 1895 (2018).

[32] Y. Kim, S. Member, and B. Toomajian, Hand gesture recognition using micro-Doppler signatures with convolutional neural network, IEEE Access **4**, 7125 (2016).

[33] B. Dekker, S. Jacobs, A. S. Kossen, M. C. Kruithof, and A. G. Huizing, Gesture recognition with a low power FMCW radar and a deep convolutional neural network, in *14th European Radar Conference* (IEEE, Piscataway, NJ, 2017), pp. 163–166.